Discover Oncology

Research

Exploring program-cell death patterns to predict prognosis and sensitivity of cervical cancer immunotherapy via multi-omics analysis and clinical samples

Chunhong Pang[1] · Xianfeng Long[3] · Yongjin Luo[1] · Ying Luo[2]

Received: 19 February 2025 / Accepted: 8 May 2025
Published online: 28 May 2025

Abstract

Background Cervical cancer (CC) progression and therapeutic resistance are driven by metastatic dissemination and immune evasion. Although immunotherapy has emerged as a promising strategy, current biomarkers fail to adequately predict patient prognosis or immune checkpoint inhibitor (ICI) responsiveness. Programmed cell death (PCD) pathways are intricately linked to tumor-immune crosstalk, yet their systematic integration into predictive models remains unexplored in CC.

Methods We constructed a prognostic gene model for PCD by mining the Cancer Genome Atlas (TCGA), GEO, and Genecards databases. The predictive capability of the model was assessed using Kaplan–Meier (K–M) analysis and Receiver Operating Characteristic (ROC) curve analysis. A nomogram was generated through Cox regression. The model was validated in both training and testing cohorts. Real-time quantitative PCR (qRT-PCR) and immunohistochemistry were used to verify the expression of the model genes. Finally, functional analysis of low- and high-risk groups based on the median risk score was performed, including immune infiltration, genomic mutations, tumor mutational burden (TMB), and drug sensitivity.

Results We established a prognostic model based on six PCD-related genes: CD46, TFRC, PGK1, GNG5, GAPDH, and PLAU. The risk score demonstrated good performance, with area under the curve (AUC) values indicating strong predictive ability (TCGA: AUC 1-year = 0.761, AUC 3-year = 0.754, AUC 5-year = 0.803; GEO: AUC 1-year = 0.702, AUC 3-year = 0.632, AUC 5-year = 0.579). Higher risk scores were associated with poorer overall survival (OS). Additionally, low-risk patients exhibited increased immune cell infiltration, higher IPS scores, enhanced expression of PDCD1 and CTLA4, and greater sensitivity to Niraparib, Paclitaxel, and Cisplatin. qRT-PCR confirmed overexpression of CD46, TFRC, PGK1, GNG5, and PLAU in cervical cancer cell lines and tissues, with consistent findings in immunohistochemistry (IHC).

Conclusion This study establishes CDI as the PCD-based immune signature for CC, enabling precise prognosis prediction and ICI candidate selection. The CDI framework provides actionable insights for combination therapies targeting PCD-immune interplay, with translational potential for personalized oncology.

Keywords Programmed cell death · Immunotherapy · Cervical cancer · Clinical verifications

Chunhong Pang and Xianfeng Long have contributed equally to this work and are co-first authors.

Supplementary Information The online version contains supplementary material available at https://doi.org/10.1007/s12672-025-02622-z.

✉ Yongjin Luo, luoyongjin951022@163.com; ✉ Ying Luo, ying_luo@gxmu.edu.cn | [1]Nanning Second People's Hospital, The Third Affiliated Hospital of Guangxi Medical University, Nanning, China. [2]Guangxi Medical University, Nanning, China. [3]Guangxi Academy of Medical Sciences, The People's Hospital of Guangxi Zhuang Autonomous Region, Nanning, China.

1 Introduction

Cervical cancer (CC), primarily squamous cell carcinoma and adenocarcinoma, is a leading cause of cancer-related deaths among women, particularly those aged 20–39 [1, 2]. Despite improved survival rates for patients with early or locally advanced CC through radical surgery or concurrent radiotherapy, prognosis remains poor for refractory cases, including recurrent, persistent, or metastatic forms [3–6]. This highlights the urgent need for new strategies to enhance outcomes for these patients.

Cell death can be categorized into accidental cell death and programmed cell death. Programmed cell death (PCD) is a cell death process mediated by a molecular program regulated by specific genes, which plays a key role in the normal development of organisms and the maintenance of homeostasis [7]. So far, at least 18 modes of PCD have been reported, such as apoptosis, necrotic death, pyroptosis, iron death, copper death, basophilic cell death, endophilic cell death, lysosome-dependent cell death, parapharyngeal cell, autophagy-dependent cell death, oxophilic cell death, basophilic cell death, and disulfide cell death [8–12]. In addition to these PCD patterns having their own unique characteristics, there is some crosstalk between some of these patterns. For example, focal death, apoptosis, and necrotic death can be induced simultaneously in the presence of sterile injury and infection [13]. Similarly, selective autophagy leads to the degradation of multiple negative regulators of cell death, thereby triggering multiple types of PCD, such as apoptosis, necrotic death, or iron death [14]. In addition, inhibition of apoptosis by caspase inhibition may activate necroptosis necrotic death pathways [15]. A growing number of studies have explored the potential role of PCD mechanisms in cancer [16]. Recent evidence also suggests that the PCD pathway is associated with the regulation of the immunosuppressive tumor microenvironment (TME) and correlates with outcomes after anticancer therapy [10]. However, the mechanism of action of PCD in cervical cancer is unclear.

In this study, PCD-related scores were calculated at the single-cell level, identifying 816 PCD score-associated genes. Using LASSO and multivariate Cox regression analyses, a prognostic model for cervical cancer was established to evaluate the impact of different Cell Death Index (CDI) levels on immune cell infiltration and responses to immunotherapy in cervical cancer patients. CDI was calculated based on the regression coefficients of model genes. The expression of these model genes was further validated in cervical cancer cell lines and clinical samples. This study highlights the potential role of PCD score-associated genes in cervical cancer, offering a promising framework for prognosis prediction and treatment stratification. The findings provide valuable insights into PCD-related biomarkers and their applications in improving therapeutic strategies for cervical cancer.

2 Methods

The flow of this article is shown in Fig. 1.

2.1 Data acquisition

RNA sequencing data and clinical details for cervical esophageal cancer (CESC) were obtained from The Cancer Genome Atlas (TCGA) database. After excluding patients with incomplete follow-up, RNA count data from 306 CESC patients and 3 normal tissue samples were analyzed. To investigate programmed cell death (PCD), a comprehensive search was performed using databases (MSigDB, GeneCards, KEGG) and relevant literature [11, 17]. A total of 1964 PCD-related genes were identified, encompassing 18 PCD subtypes, including apoptosis (580 genes), pyroptosis (52), ferroptosis (88), autophagy (367), necroptosis (101), cuproptosis (19), parthanatos (9), endogenous cell death (15), eosinophil cell death (8), lysosome-dependent cell death (220), alkaliptosis (7), oxytosis (5), neutrophil extracellular trap-associated cell death (24), immunogenic cell death (34), anoikis (338), paraptosis (66), large-scale apoptotic cell death (8), and intracellular engulfment-related cell death (23). Details are provided in Supplementary Table S1. Single-cell data were derived from previous literature, including 5 patients with cervical cancer [18].

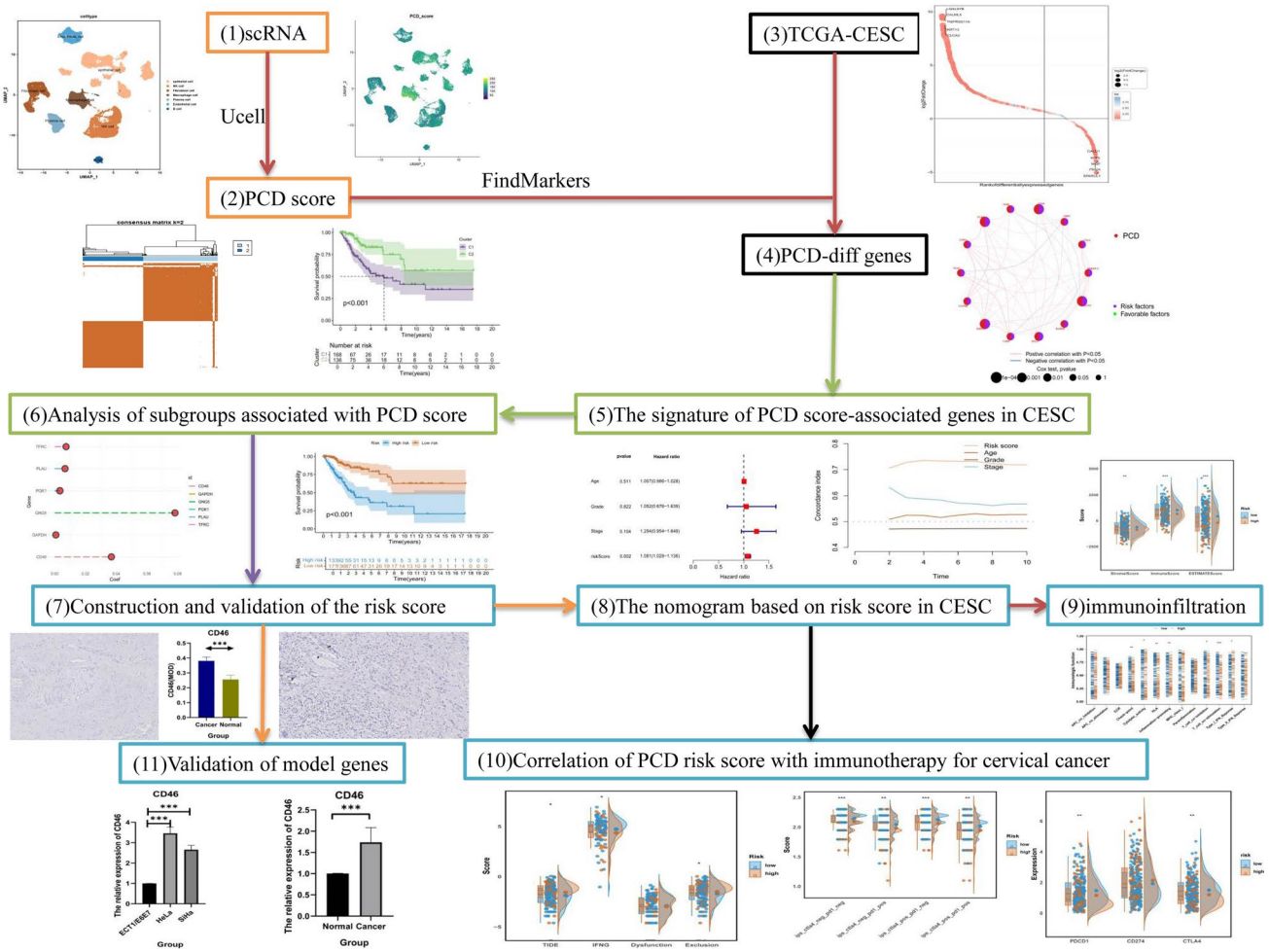

Fig. 1 Flowchart of this study. Distinct colors were used to represent different analytical stages and outcomes. Single-cell RNA sequencing data is highlighted in orange, while TCGA differential analysis and prognostic gene screening are denoted with black borders. Light green signifies the construction of the prognostic model, and blue represents comprehensive validation of the model across multiple aspects

2.2 ScRNA-Seq data preprocessing and analysis

Single-cell RNA sequencing (scRNA-seq) datasets were processed separately using Seurat v4. Genes with expression levels ranging from 200 to 6000 were selected, ensuring mitochondrial gene scores were below 10%. Following gene selection, data were normalized using "NormalizeData," and the top 2000 highly variable genes (HVGs) were identified to stabilize UMI count variances. Batch effects were then corrected using Harmony, and cell cycle effects were adjusted. PCA-based data clustering using PC 40 and a resolution of 0.02 identified seven clusters characterized by typical cell type marker genes. Notable markers included PTPRC and CCL5 for natural killer (NK) cells, S100 A8 and KRT19 for epithelial cells, COL1 A1 and ACTA2 for fibroblasts, SPP1 and LYZ for macrophages, IGHG1 and IGKC for mast cells, VWF and PLVAP for endothelial cells, and MS4 A1 and CD79 A for B cells. Bubble plots visualized marker gene expressions across cellular subpopulations. This collection was scored using UCell methods, and average scores were calculated. Cells were categorized into high PCD score and low PCD score groups based on median average scores. Differential gene expression analysis was then performed between these groups.

2.3 Differential expression analysis

Differential expression analysis was conducted using the Limma package in R. Genes were considered significant if they met the criteria of adjusted *p* value <0.05 and |log fold change| > 1. Univariate Cox regression analysis (Survival package v3.5-5) was applied with a stringent *p* value threshold of <0.01 to ensure statistical robustness. This identified genes with strong individual prognostic value. This multi-criteria approach yielded 14 high-confidence prognostic genes while minimizing false positives. The Cox models incorporated survival time, patient status, and normalized gene expression values throughout all analyses.

2.4 Characterization of genes associated with PCD genes

We identified a set of prognostic genes associated with PCD genes. We conducted network localization analysis to investigate their prognostic implications in cervical cancer patients. This analysis encompassed the assessment of somatic mutation frequencies, genetic loci, and copy number variations (CNVs) affecting these genes. To validate our findings, we performed one-way Cox regression analysis using data from the GSE44001 cervical cancer dataset.

2.5 Molecular subtyping

Cluster analysis of CESC patients was conducted based on RNA sequencing data of 14 prognostic genes in cervical cancer tissues. Utilizing the *K*-means algorithm from the "Consensus Cluster" R package, consistent clustering was achieved through 50 repetitions to ensure robust subtype identification. The optimal number of subclusters was determined using metrics such as Consistency Cumulative Distribution Function (CDF), delta area, and Cluster Consistency (CLC). In the TCGA cohort, CESC patients were stratified into two subtypes based on consistent clustering of these prognostic genes. Survival analysis comparing these subtypes was performed using Kaplan–Meier curves and the "Survival" R package. Additionally, Gene Ontology (GO) enrichment and KEGG pathway analyses were conducted using the "ClusterProfiler" R package to elucidate the biological processes and pathways associated with each molecular subtype. The infiltration levels of immune cells and immune scores in cervical cancer patients were assessed using single-sample gene set enrichment analysis (ssGSEA) and ESTIMATE algorithms, respectively, and were compared between the identified subtypes.

2.6 Generation of the PCD prognostic signature

Subsequently, integrating expression data of differentially expressed genes with clinical information, we divided the TCGA dataset into train and validation sets in a 6:4 ratio. We performed multifactorial Cox regression analysis on the TCGA-train set, TCGA-test set, GEO set, and the TCGA cohort to develop a prognostic model based on six PCD-related genes significantly associated with overall survival (OS). The risk score for this model was calculated using the risk coefficients of the six genes: Cell Death Index (CDI) = $\Sigma(C_i * E_i)$. In this context, (C_i) represents the coefficients derived from the multivariate Cox regression analysis for each feature, while (E_i) denotes the expression value of each feature. Based on the median CDI, patients were categorized into high-risk and low-risk groups. To assess the accuracy and sensitivity of the model, we employed the "timeROC" package (version 0.4) in R to plot time-dependent receiver operating characteristic (ROC) curves. Additionally, we used the "survival" package to generate survival curves for different datasets, which allowed us to evaluate the prognostic differences between the risk groups.

2.7 Nomogram construction and characteristic of risk score model

Univariate and multivariate Cox regression analyses were conducted using the "Survival" software package to examine the associations between CDI and clinical characteristics. Subsequently, risk scores and clinical data were integrated to generate line plots using the "RMS" software package. Both nomograms and risk score models were assessed using

calibration curves and ROC curves. Furthermore, comparisons were made between the high-risk and low-risk groups regarding clinical characteristics, tumor stem cell index, and immune score.

2.8 Analyses of relation between tumor mutation burden, tumor stemness indices, and risk score and prediction of the effective response of postoperative immunotherapy

Immune cell infiltration levels between the two risk groups were assessed using ssGSEA and the "CIBERSORT" software package. The TIDE algorithm was then employed to evaluate response to immune checkpoint blockade (ICB) therapy and predict neoantigenic activity. Higher TIDE scores indicate increased immune evasion mechanisms such as T-cell dysfunction and rejection, correlating with poorer immunotherapy response. Immunotherapy scores for the large sample cohort from the TCGA database were obtained using TCIA, comparing treatment responses to anti-CTLA4 and anti-PD1 inhibitors across different risk groups. CNVs were analyzed using GISTIC, and mutation frequencies were calculated from somatic mutation data (processed using MuTect2 variant aggregation and masking) sourced from the TCGA-CESC dataset via the "maftools" R package. Tumor Mutation Burden (TMB), defined as the number of mutations per million bases in somatic cells, was also assessed using "maftools". Kaplan–Meier (KM) analysis was performed to evaluate differences in OS across TMB groups.

2.9 Correlation of drug sensitivity and risk score

Initial comparisons of survival disparities and immunotherapy responses among different risk groups utilized the IMvigor210 dataset. Additionally, survival differences across risk groups were assessed in the GSE78220 and GSE135222 datasets, while treatment sensitivity was evaluated using the GSE91061 dataset. Furthermore, the correlation between risk scores and IC50 values for commonly used chemotherapeutic agents (such as cisplatin, adriamycin, and paclitaxel) and targeted therapies was analyzed. IC50 data for these drugs were sourced from the Genomics of Drug Sensitivity in Cancer (GDSC) database.

2.10 Cell culture

Cervical cancer cells (HeLa and SiHa) and normal cervical epithelial cells (ECT1/E6E) were kindly donated to Li Li's group at the Cancer Hospital of Guangxi Swell Medical University. These cells were maintained in RPMI 1640 medium (Sigma–Aldrich; Thermo Fisher Scientific) containing 10% fetal bovine serum (FBS) (FBS; Gibco; Expression Vector; Thermo Fisher Scientific), 100 IU/mL penicillin and 10 µg/mL streptomycin (Thermo Fisher Scientific). All cells were cultured at 37 °C under 5% CO2.

2.11 Clinical sample acquisition

A total of 10 cases of fresh cervical cancer tissues and 10 cases of fresh normal cervical tissues were collected in the Nanning Second People's Hospital from 2023 to 2024. Written informed consent was obtained from each patient and approved by the Research Ethics Committee of the Nanning Second People's Hospital. The Experimental Procedures section that the studies in this work abide by the Declaration of Helsinki principles.

2.12 qRT-PCR analysis

These RNAs were extracted by TRIzol® (Invitrogen; Thermo Fisher Scientific, Inc.) and reverse transcribed by HiScript III RT SuperMix for qPCR (Vazyme Biotech). Gene primer sequences are shown in Table S2. PCR cycling parameters were: 95 °C for 5 min, 40 cycles of 30 s, and 60 °C for 1 min. each sample was performed in 3 separate reactions, and the average of each point was calculated. mRNA expression levels were normalized to GAPDH levels.

2.13 Immunohistochemistry

Tissue specimens were routinely fixed in 4% paraformaldehyde, paraffin-embedded, and sliced to 3.5 µm thickness. For ICH analysis, these sections were first dehydrocarbonized in xylene, then rehydrated to water by a series of 100–50% ethanol solutions, and then immersed in 0.01 mol/L orange hydrochloric acid nano-buffer (pH = 6.0), and heated in a

water bath for antigen recovery. After inactivation of endogenous peroxidase activity in 3% H_2O_2 solution and blocking in 10% goat serum to minimize any potential nonspecific reaction with the secondary antibody, the sections were incubated overnight at 4 °C with anti-CD46, GNG5, PLAU, TFRC and PGK1 antibodies (Affinity, Jiangsu, China). On the following day, sections were incubated with horseradish peroxidase (HRP)-coupled secondary antibody (ZSGB-BIO, Beijing, China) for 1 h at room temperature, visualized with 3,3-diaminobenzidine (DAB) solution (ZSGB-BIO), and counterstained with hematoxylin. After fixation with cover slips, immunostained sections were examined and scored under a computerized image processing system (Olympus, Tokyo, Japan) and software analysis (Media Cybernetics, MD, USA). The immunopositive staining area was selected and the intensity and area of immunopositive staining were calculated by human–computer interaction. Mean optical density (MOD) = integrated optical density (IOD)/total image area.

2.14 Statistical analysis

All statistical analyses in this experiment were conducted using R version 4.3. For non-parametric data, the Wilcoxon test and Kruskal–Wallis test were employed to compare two independent samples and multiple samples, respectively. Parametric data were analyzed using the *t* test and one-way ANOVA. Statistical significance was defined as a *p* value <0.05 (* $p < 0.05$; ** $p < 0.01$; *** $p < 0.001$). Relevant R packages, including "ggplot2", "ggpubr", "survival", "survminer" and others, were obtained from Bioconductor or CRAN repositories. The threshold for statistical significance was consistently set at $p < 0.05$ for all analyses.

3 Result

3.1 Analysis of PCD associated with cervical cancer single cells

Using single-cell analysis, we performed rigorous quality control and filtering to obtain high-quality transcriptomic data from 48,045 cells. We assessed the enrichment of PCD-related genes by scoring these data. To mitigate batch effects and reduce variability in cell distribution, we employed Harmony for batch correction (Fig. 2A). Subsequently, we conducted PCA clustering, which identified seven distinct clusters with minimal inter-cluster overlap (Fig. 2B). Cell annotation based on marker genes categorized these clusters into epithelial cells, endothelial cells, fibroblasts, macrophages, B cells, plasma cells, and NK cells (Fig. 2C). A bubble plot illustrated the expression of marker genes across different cell subpopulations, highlighting distinct expression patterns (Fig. 2D). We calculated PCD scores for PCD-related genes using the UCell scoring method and mapped these scores onto boxplots. This analysis revealed a predominant enrichment of PCD scores in macrophages (Supplementary Fig. S1). We then computed the average scores for 18 distinct PCD patterns, with results visualized through UMAP plots showing cell distribution (Fig. 2E). Notably, high expression of specific PCD patterns was observed, as detailed in Fig. 2F and G. Cells were classified into high and low PCD score subgroups based on the median PCD score. Differential gene expression analysis was subsequently performed to compare these subgroups.

3.2 The signature of PCD score-associated genes in CESC

Among the 816 PCD-related genes analyzed, 353 exhibited significant differential expression in cervical cancer, with 53 genes being downregulated and 300 genes upregulated (Fig. 3A). A univariate Cox regression analysis of these 353 genes identified 14 that are associated with cervical cancer prognosis (Fig. 3B). To elucidate the complex relationship between PCD-related genes and cervical cancer prognosis, a network diagram was constructed (Fig. 3C). The somatic mutation frequencies of these 14 genes in cervical cancer were examined, revealing that DSG2 had the highest mutation rate, reaching up to 15%, while the other genes showed relatively low mutation frequencies (Fig. 3D). The genomic locations of these 14 genes are depicted in Fig. 3E. Further analysis uncovered widespread CNVs among these genes, with FDPS and TFRC showing amplifications, and GNG5 exhibiting deletions (Fig. 3F). Comparative analysis indicated that most PCD-related genes were significantly upregulated in cervical cancer tissues compared to normal tissues (Fig. 3G). To assess the impact of these 14 genes on OS in cervical cancer patients, data from the GEO dataset were utilized. The analysis demonstrated that the expression levels of SERINC2, GNG5, PGK1, LDHA, and DSG2 were statistically significantly associated with OS (Fig. 3H).

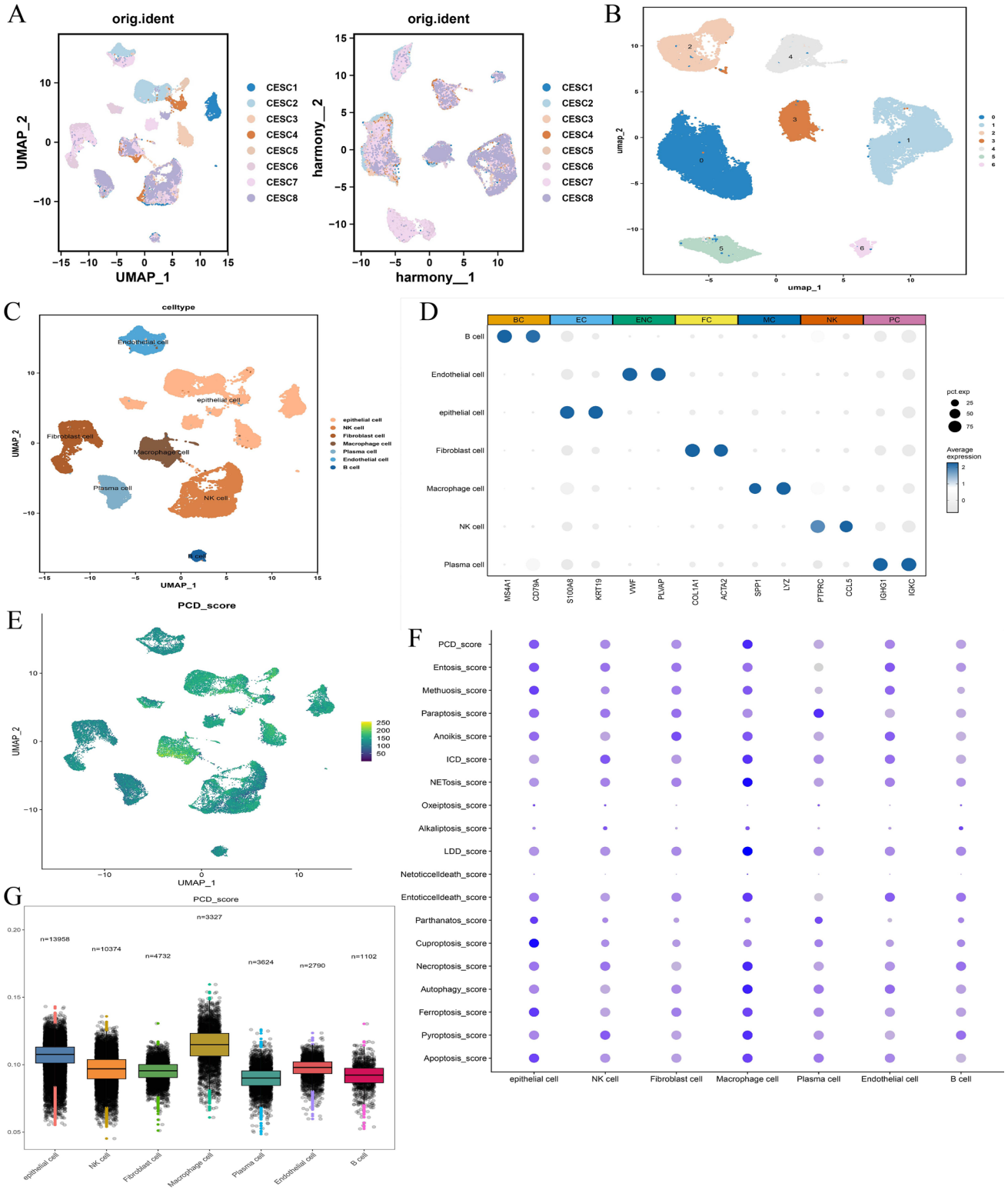

Fig. 2 Single-cell analysis of PCD-associated differential genes. **A** Cell distribution map of samples after harmony. **B** Umap plot of single-cell clusters. **C** Umap plot of cell subpopulations after annotation. **D** Bubble plot of marker genes for different cell subpopulations. **E** Umap of PCD scores. **F** 18 kinds of PCD mode rating and PCD rating bubble chart. **G** RA-associated scores box plots for different cell subpopulations

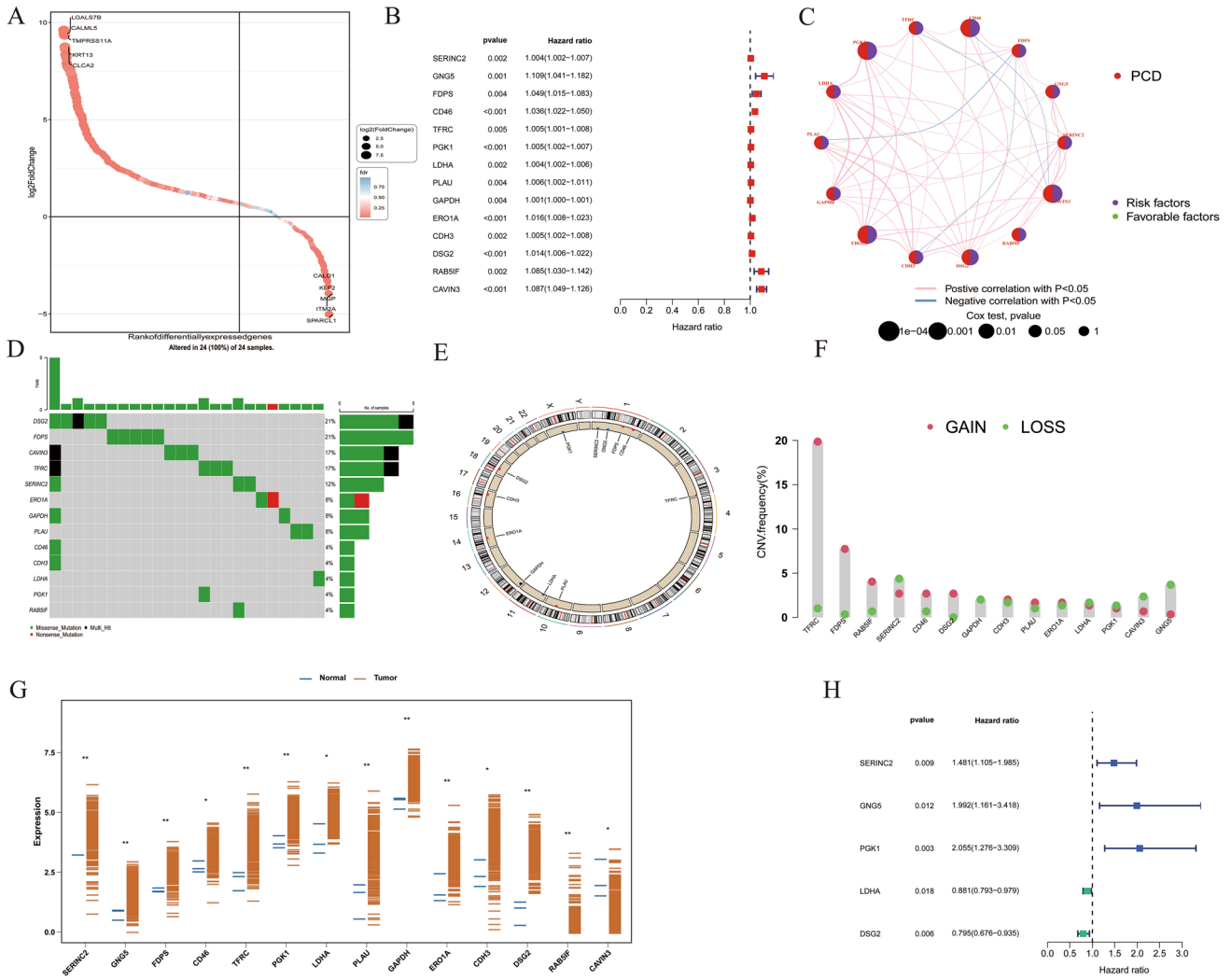

Fig. 3 Genetic variation and expression of PCD-associated scoring genes in cervical cancer. **A** The differences of PCD-associated scoring genes genes on TCGA cervical cancer. **B** The prognostic forest plot of 14 PCD scoring-associated genes in cervical cancer. **C** Network diagram showing the interaction of 14 PCD score-related genes in cervical cancer. **D** Mutation rates of the top 10 prognostically relevant PCD score genes in cervical cancer. **E** Localization of the 14 PCD score-related genes on 23 chromosomes. **F** Frequency of CNV mutations of the 14 PCD score-related genes in TCGA-CESC. **G** Differential expression of the 14 PCD-score-related genes between normal tissues and cervical cancer. **H** Forest map of cervical cancer prognostic related PCD gene in GSE44001 dataset. * denotes $p < 0.05$; ** denotes $p < 0.01$; *** denotes $p < 0.001$; ^{ns} denotes $p > 0.05$

3.3 Analysis of subgroups associated with PCD score

Based on the expression matrix of the eight prognostic genes, consensus clustering analysis divided 304 cervical cancer patients into two groups: C1 and C2 (Table S3), as illustrated in Fig. 4A–C. The expression differences of the eight genes between the C1 and C2 clusters are shown in Fig. 4D. Kaplan–Meier (KM) analysis revealed a significant difference in survival rates between the C1 and C2 groups ($p = 0.001$) (Fig. 4E). Regarding TME differences, C2 demonstrated higher infiltration of various immune cells, including regulatory T cells, CD8 T cells, activated NK cells, and dendritic cells (Fig. 4F). Immune scoring of cervical cancer tissues indicated that C2 had markedly higher immune, stromal, and ESTIMATE scores (Fig. 4G). Additionally, Gene Set Enrichment Analysis (GSEA) revealed that the C1 subtype was predominantly enriched in tumor-associated signaling pathways, such as the TP53 pathway and the Hippo pathway (Fig. 4H). KEGG pathway analysis highlighted significantly activated pathways in C2, such as BIOSYNTHESIS_OF_UNSATURATED_FATTY_ACIDS and ADHERENS_JUNCTION (Fig. 4I). Finally, Gene Ontology (GO) biological pathway analysis showed significant enrichment of functional groups in C2, including

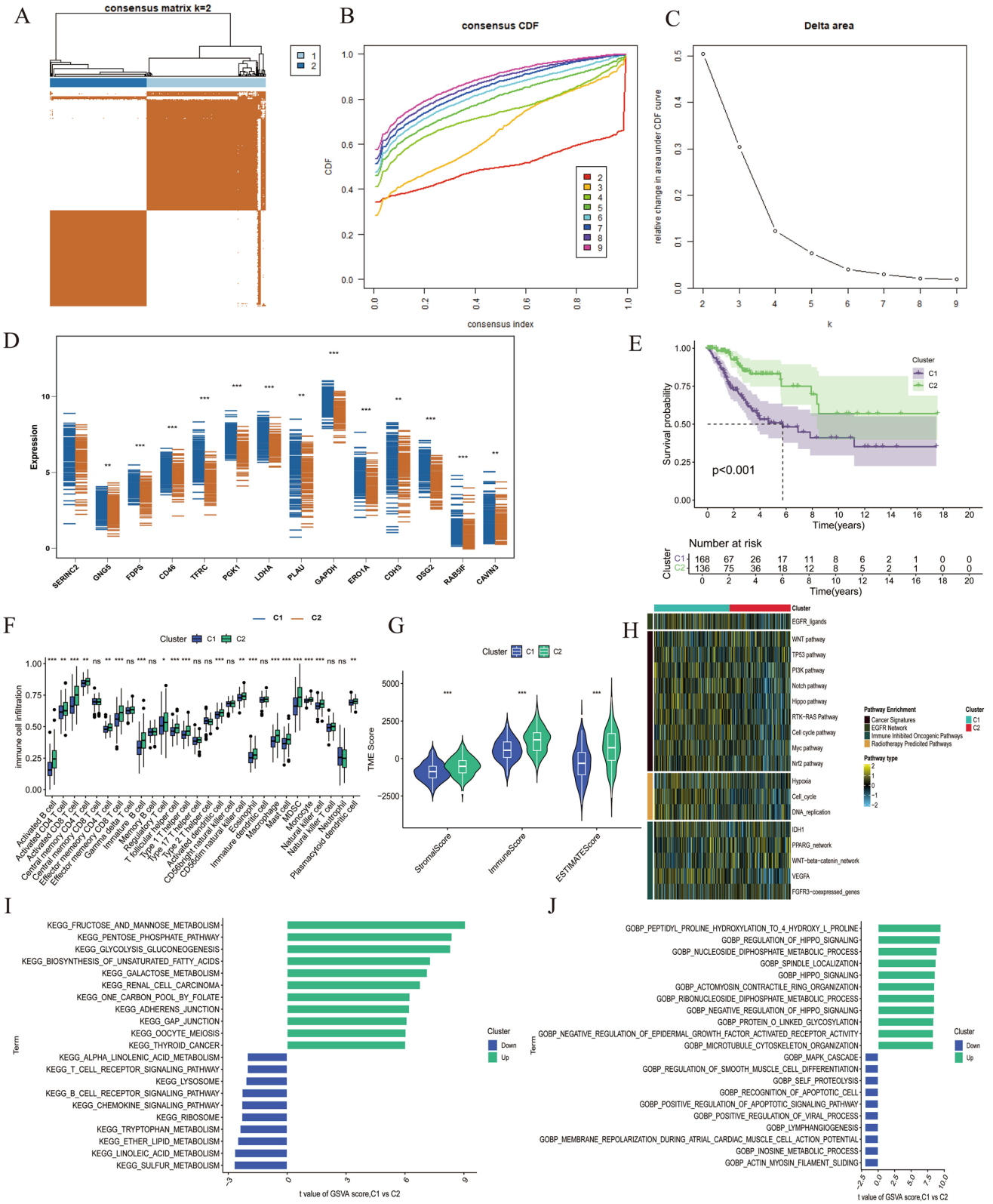

Fig. 4 Correlation of PCD score-related patterns with TME and clinical characteristics. **A**–**C** Cervical cancer patients were categorized into two distinct gene clusters (C1 and C2) using ConsensusClusterPlus. **D** Differential analysis of 23 PCD score-related genes in C1 and C2. **E** Survival analysis of the C1 and C2 cohorts ($p = 0.001$). **F** Differential analysis of 28 immune cell infiltrates. **G** Estimate, stromal score and immune score in C1 and C2 cohorts. **H**–**J** GSEA, KEGG and GO analyses revealed enrichment in two PCD subtypes. (* $p < 0.05$; ** $p < 0.01$; *** $p < 0.001$)

PEPTIDYL_PROLINE_HYDROXYLATION_TO_4_HYDROXY_L_PROLINE and REGULATION_OF_HIPPO_SIGNALING (Fig. 4J).

3.4 Construction and validation of the CDI model

LASSO regression analysis of the eight genes selected seven for further investigation (Fig. 5A, B). The TCGA dataset was divided into training ($N = 183$) and validation ($N = 121$) sets in a 6:4 ratio, with clinical characteristics detailed in Table S4. A multifactorial Cox regression analysis was conducted to develop a prognostic model for cervical cancer patients, incorporating the genes GAPDH, PLAU, TFRC, GNG5, PGK1, and CD46 (Fig. 5C). Using the median CDI, patients in the TCGA-train, TCGA-test, TCGA, and GEO cohorts were classified into high-risk and low-risk groups (Table S5). Across all datasets, patients in the low-risk group demonstrated significantly better overall survival (OS) compared to the high-risk group ($p < 0.05$, Fig. 5D–G). Additionally, the relationship between model genes and cervical cancer prognosis was further explored (Supplementary Fig. S2). Finally, ROC curves were analyzed for 1-year, 3-year, and 5-year survival predictions across different datasets. Notably, the 1-year Area Under the Curve (AUC) for the TCGA-train, TCGA-test, TCGA, and GEO cohorts were 0.784, 0.740, 0.761, and 0.702, respectively; the 3-year AUCs were 0.803, 0.734, 0.754 and 0.632; and the 5-year AUCs were 0.803, 0.832, 0.803, and 0.579 (Fig. 5H–K).

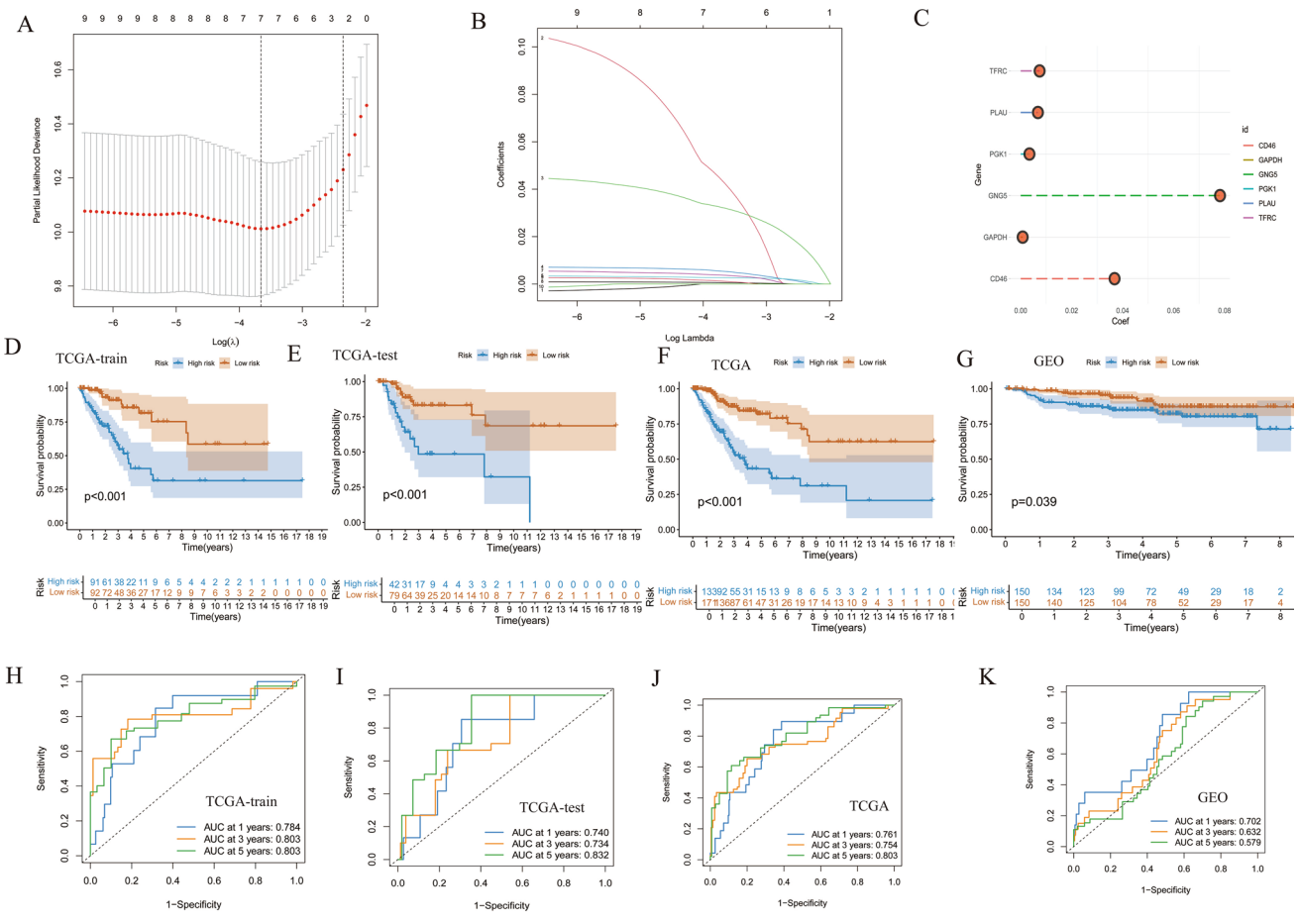

Fig. 5 Development and validation of CDI by lasso and multivariate Cox regression analysis. **A**, **B** Lasso regression analysis results. **C** Prognostic model gene regression coefficient diagram. **D**–**G** Kaplan- for OS of cervical cancer patients based on CDI from the TCGA training set, the TCGA internal validation set, the TCGA cohort, and GEO. **H**–**K** ROC curves for OS calculated from risk scores in TCGA training set, TCGA internal validation set, TCGA cohort and GEO

3.5 The nomogram based on CDI in CESC

To investigate the independent prognostic value of cervical cancer risk scores relative to other clinical features such as age, grade, and stage, both univariate and multivariate Cox regression analyses were performed. These analyses revealed that risk scores independently predicted overall survival (OS) in cervical cancer, with hazard ratios of 1.106 (95% CI, 1.061–1.154) and 1.081 (95% CI, 1.029–1.136) (Fig. 6A, B). Nomogram plots were constructed using TCGA data to predict 1-year, 3-year, and 5-year OS, incorporating risk scores, age, grade, and stage as predictive parameters (Fig. 6C). The nomogram demonstrated high predictive accuracy, with 1-year, 3-year, and 5-year survival rates of 82.2%, 38.2%, and 27.2%, respectively. Calibration curves for 1-year, 3-year, and 5-year OS indicated a good alignment between predicted and actual outcomes (Fig. 6D). Furthermore, the risk score had the highest concordance index (c-index), exceeding 0.7, indicating robust prognostic performance (Fig. 6E). Decision curve analysis (DCA) reinforced the utility of risk scores as a prognostic tool, highlighting their effectiveness across 1-year, 3-year, and 5-year predictions (Fig. 6F; Supplementary Fig. S3). ROC curves combining clinical features demonstrated that the risk score outperformed other variables at 1, 3, and 5 years, with AUCs of 0.761, 0.754, and 0.803, respectively (Fig. 6G; Supplementary Fig. S3). A heatmap revealed

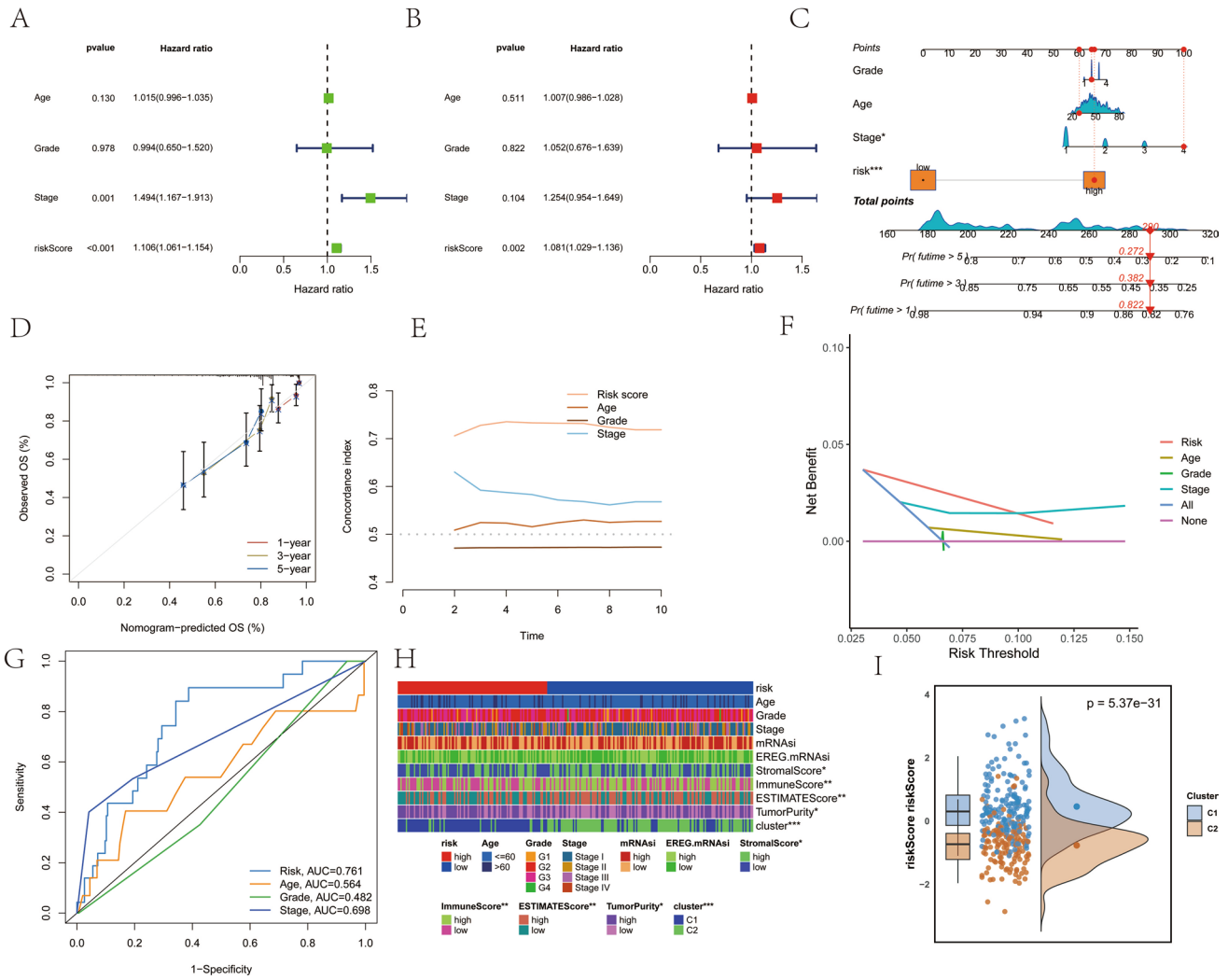

Fig. 6 Construction and validation of the nomogram. **A**, **B** Univariate and multivariate analyses of clinical characteristics and CDI. **C** Construction of the nomogram based on risk scores and clinical characteristics, including age, grade, stage, and CDI. **D** Correction curves for the 1-, 3-, and 5-year OS nomogram. **E** Comparison of the risk scores with the C-index for the other clinical characteristics. **F** Decision-curve analysis (DCA) showing 1-year net benefits by applying the nomogram and other clinical characteristics to show 1-year net benefit. **G** ROC curves showing the predictive performance of 1-year risk scores and clinical characteristics. **H** Heat maps of risk scores versus different clinical characteristics, cluster subgroups, and immune-related scores. **I** Violin plot of risk score between C1 and C2

significant clustering differences between risk groups in terms of stage, immune scores, and stromal scores (Fig. 6H). Analysis of risk score differences among clusters with varying PCD-related scores showed that the C2 subgroup had a lower risk score (Fig. 6I).

3.6 Correlation between CDI and immune cell infiltration in cervical cancer

In the low-risk group, the expression of most HIL family genes was elevated (Fig. 7A). Various methods, including ssGSEA, were employed to enrich and analyze immune cells and their functions. The analysis revealed that many immune functions, such as checkpoint and T_cell_co_inhibition, were significantly enriched in the low-risk group (Fig. 7B). Figure 7C demonstrates that compared to the high-risk group, the low-risk group exhibited more pronounced infiltration of immune cells, including Activated CD8 T cells, Activated B cells, and mast cells. Immune scoring also indicated that the low-risk group had higher immune, ESTIMATE, and stromal scores (Fig. 7D). Additionally, results from the CIBERSORT algorithm showed more pronounced infiltration of various immune cells, particularly CD8 T cells, in the low-risk group (Fig. 7E).

3.7 Correlation between immunotherapy efficacy and CDI in cervical cancer

Immunotherapy is emerging as a treatment option for advanced cervical cancer. Analysis of TIDE results indicated that the immune response rate in the low-risk group (39%) was higher than that in the high-risk group (35%) (Fig. 8A). Additionally, the low-risk group exhibited lower tumor immune dysfunction and rejection scores, whereas

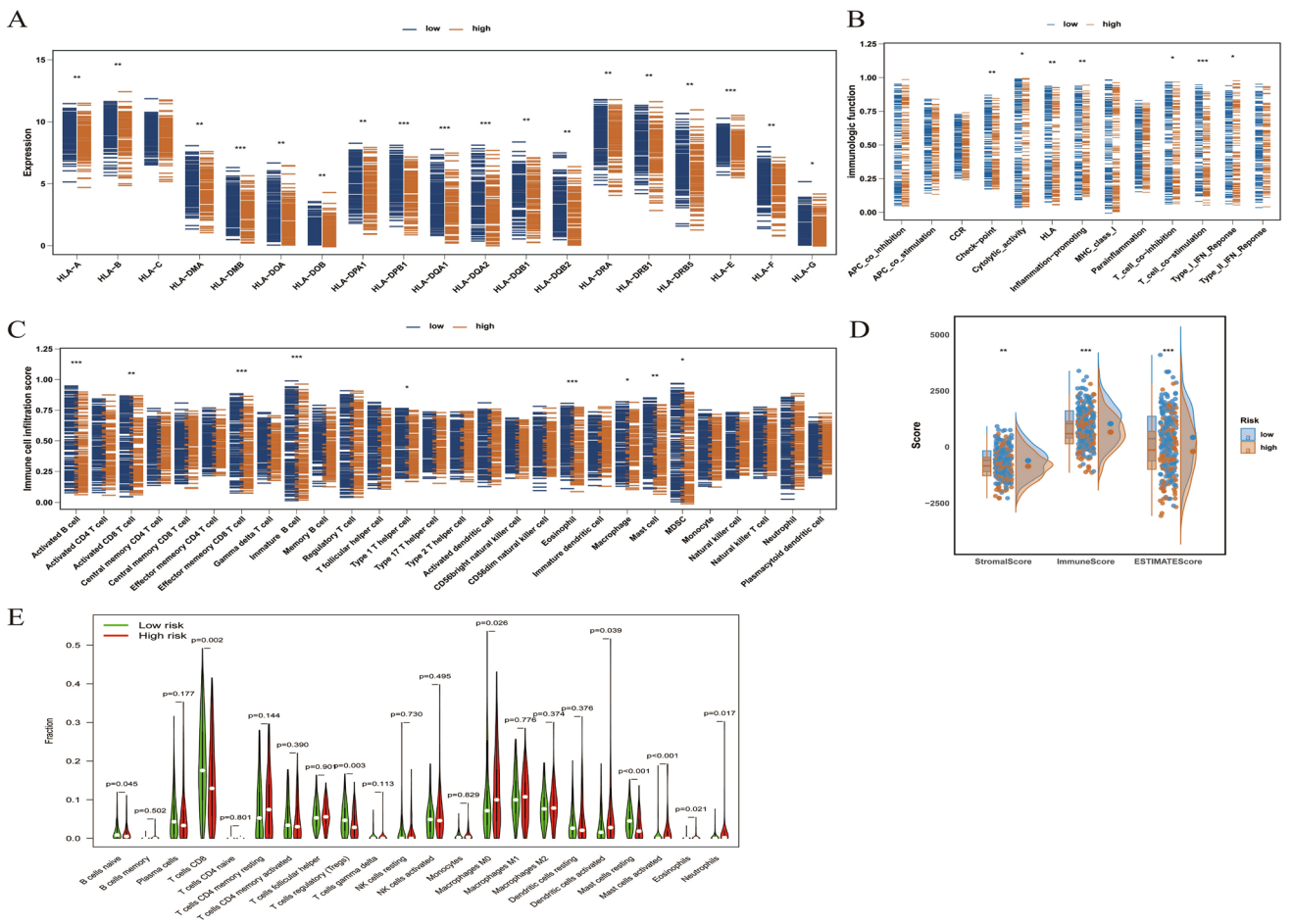

Fig. 7 Relationship between CDI and immune cell infiltration and immune-related genes. **A** Differential analysis of risk scores and HLA-related genes. **B** Differential analysis of immune function between different risk scores. **C** Comparison of ssGSEA immune cell infiltration levels between different risk scores. **D** Comparison of immune scores between different risk scores. **E** Differential analysis of CIBERSORT-associated immune cells between different risk scores

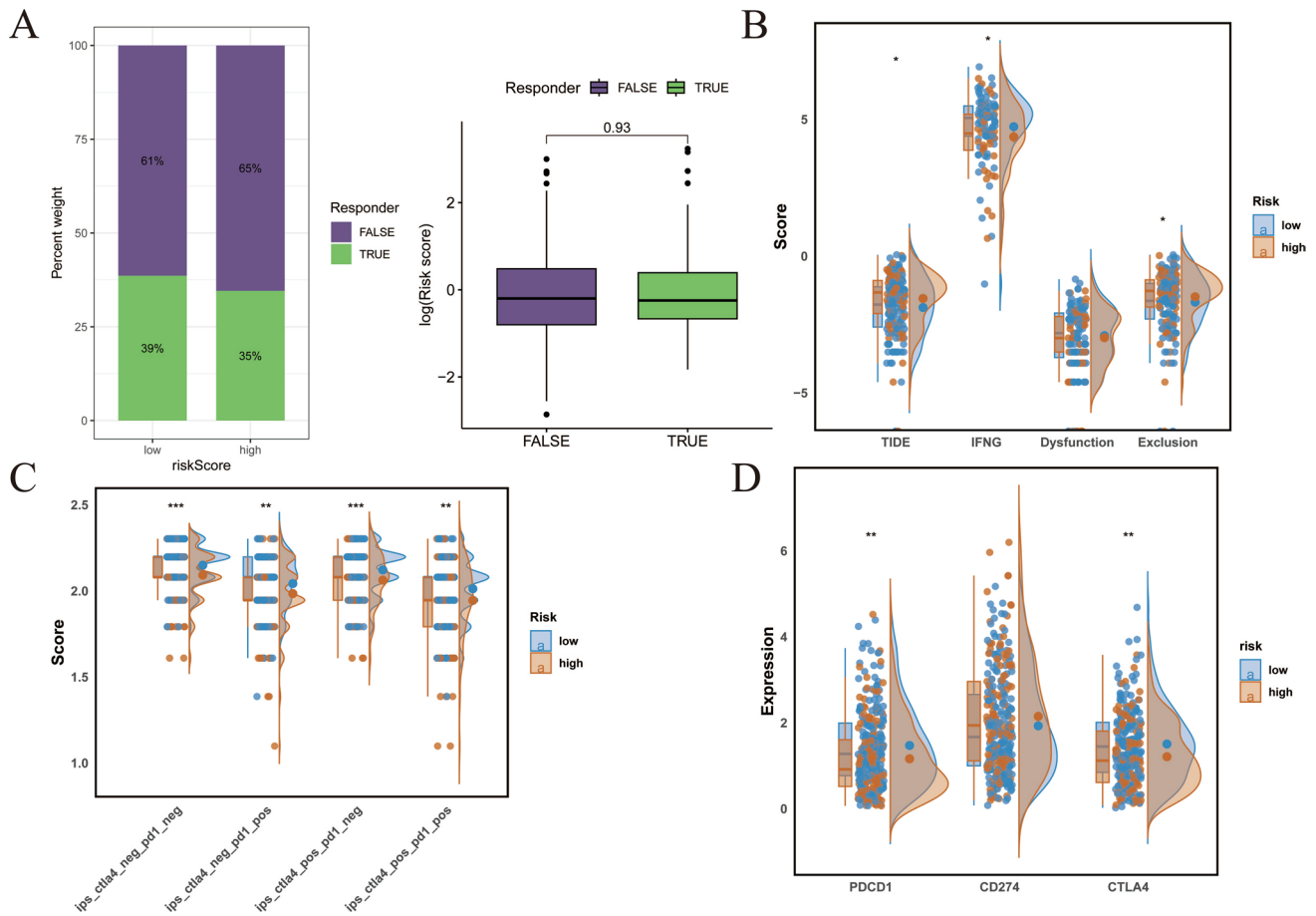

Fig. 8 Correlation of different risk scores with immune checkpoint-associated genes and sensitivity to immunotherapy. **A** Differences in immune response between risk groups. **B** IFNG score, TIDE score, dysfunction score and exclusion score assessed for different risk scores. **C** Analyze the differences in IPS scores between risk scores. **D** Differences in 3 immune checkpoint-associated genes between risk scores

dysfunction and interferon-gamma scores showed an inverse trend (Fig. 8B). Given the potential efficacy of immune checkpoint inhibitors (ICIs) in blocking CTLA4/PD-1 interactions for treating certain tumors, IPS scores were utilized to assess treatment potential based on IFNG expression levels. Notably, patients in the low-risk group demonstrated higher IPS scores across multiple assessments (Fig. 8C). Figure 8D highlights significant differences in checkpoint gene expression between the two groups, with the low-risk group showing higher expression levels. This includes several well-known immunotherapy targets, such as PDCD1 (PD-1), CD274 (programmed death ligand 1, PD-L1), and CTLA4.

3.8 Correlation of somatic mutations and CDI in cervical cancer

Tumor mutations significantly impact patient prognosis. As shown in Fig. 9A and B, the mutation frequencies in the low-risk group (86.08%) was higher than the high-risk group (82.54%). Analysis of the mutated genes in these subgroups revealed consistency in the top five mutated genes between the two groups. Comparison of tumor mutation burden (TMB) values across different risk score groups indicated that patients in the low-risk group had higher TMB values, although the difference was not statistically significant (Supplementary Fig. S4). Figure 9C and D illustrate the CNV values between high and low-risk groups. Additionally, Fig. 9E shows that patients with high TMB had better survival rates compared to those with low TMB. Furthermore, Fig. 9F indicates that the high-risk group and the low TMB group exhibited the poorest prognosis.

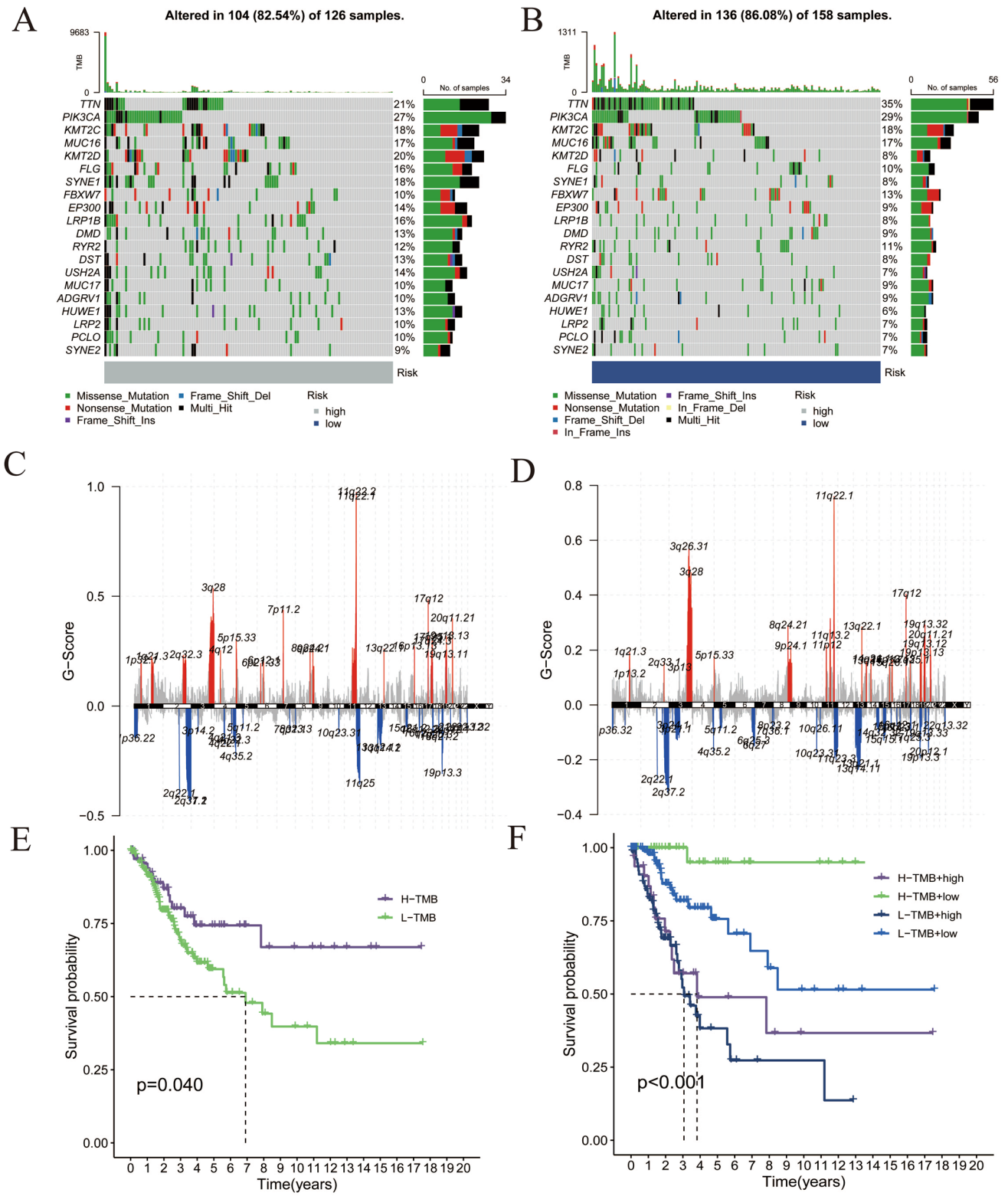

Fig. 9 Relationship between different risk scores and somatic mutations. **A** Mutation information of the low risk group. **B** Mutation information of the high-risk group. **C**,**D** The CNV of patients in low risk group and high risk group, respectively. **E**, **F** Prognostic survival curves of TMB combined with different risk scores in patients with cervical cancer

3.9 CDI provide excellent prediction of immunotherapy response and drug treatment

In the IMvigor-210 cohort, the restricted mean survival (RMS) at 6 and 12 months was compared between the two patient groups to elucidate the delayed clinical effects of immunotherapy and to assess long-term survival differences at 3 months post-treatment ($p < 0.05$; Fig. 10A, B). The results indicated that patients in the low-risk group had better prognoses, suggesting a greater benefit from immunotherapy. Additionally, the distribution of risk scores among patients with different treatment responses showed that the response group (complete remission [4]/partial remission

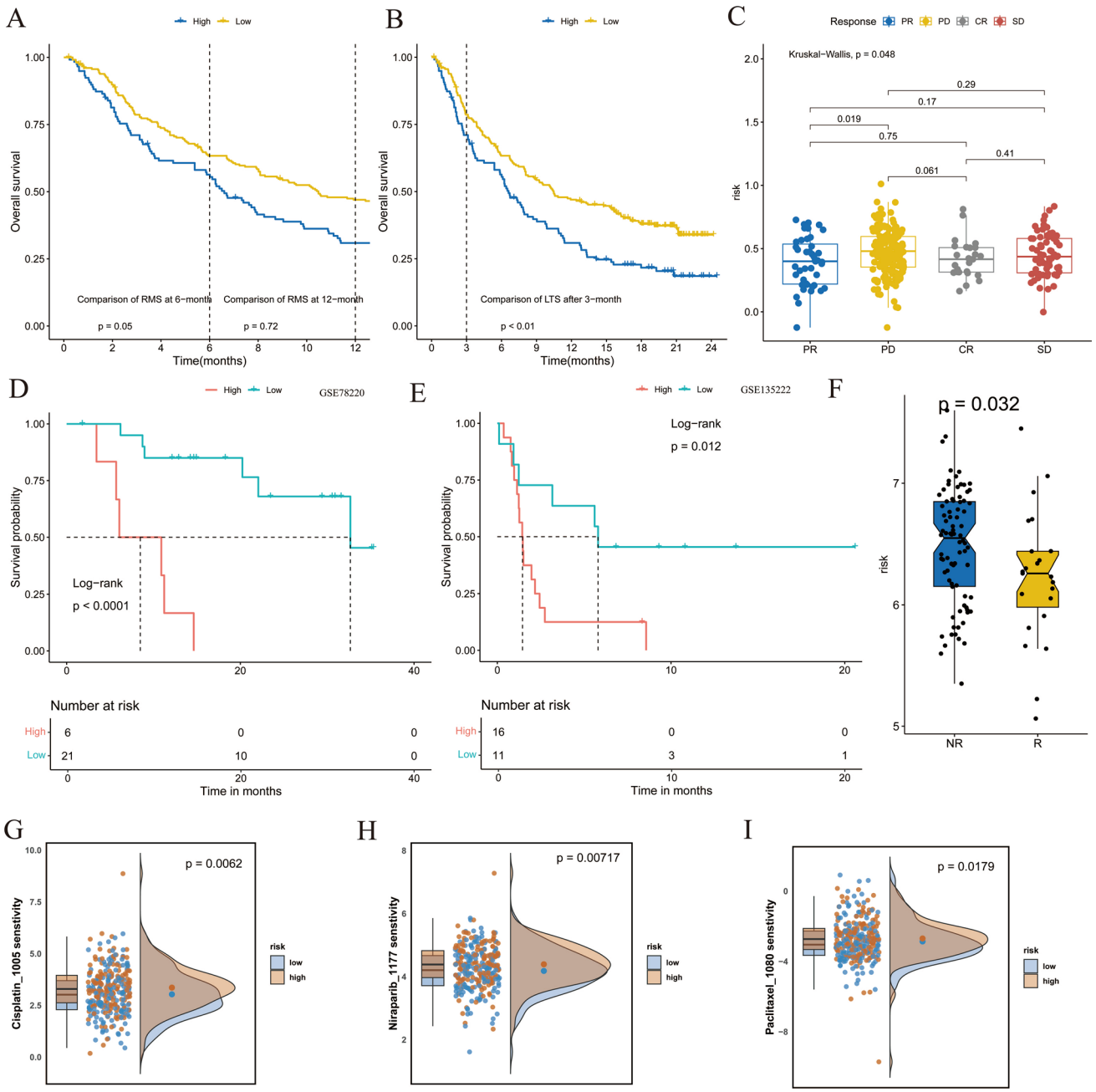

Fig. 10 Value of risk scores in predicting response to immunotherapy. **A** Difference in restricted mean survival (RMS) time at 6 months and 1 year after treatment between high- and low-risk groups. **B** Difference in long-term survival (LTS) after 3 months of treatment between high- and low-risk groups. **C** Distribution of risk scores in different immunotherapy response groups. **D** Survival analysis of high- and low-risk groups in GSE78220. **E** Survival analysis of high- and low-risk groups in GSE135222. **F** Distribution of risk scores in different immunotherapy response groups in GSE91061. **G**–**I** IC 50% values for cisplatin, niraparib, paclitaxel between high and low risk groups, respectively

[19]) had significantly lower risk scores compared to the non-response group (progressive disease [PD]/stable disease [SD]) ($p = 0.43$; Fig. 10C). These findings were validated across multiple immunotherapy cohorts with prognostic information. Similarly, the low-risk group exhibited better post-immunotherapy outcomes in GSE78220 ($p < 0.0001$) (Fig. 10D) and GSE135222 ($p = 0.012$) (Fig. 10E), and showed superior immunotherapy results in GSE91061 ($p = 0.032$; Fig. 10F). Finally, the IC50 values for drugs such as cisplatin, niraparib and paclitaxel were compared, consistently revealing that the low-risk group had lower IC50 values. This suggests that patients in the low-risk group are more sensitive to these medications (Fig. 10G–I).

3.10 Validation of model gene expression in cervical cancer

Figure S5 shows that in TCGA cervical cancer data, the protein expression levels of model gens are relatively high using the HPA protein database. What`s more, validation through the GEPIA 2 online database and ualcan database further confirmed the high expression of these genes in cervical cancer tissues (Figs. S6, S7). This trend was also confirmed in cervical cancer cell lines (Fig. 11A). Additionally, in clinical tissue samples, the RNA and protein expression of these genes were higher in the cancer tissues compare the normal tissues (Fig. 11B–D).

4 Discussion

Immunotherapy, as a key treatment strategy for patients with advanced cervical cancer, has the potential to prolong survival [20]. However, the efficacy of immunotherapy in cervical cancer patients varies and may depend on TME and immune activity [19, 21, 22]. With the continued study of PCD in tumors, PCD has been found to play an increasingly critical role in tumorigenesis, progression, and treatment [10], and is now clearly and significantly correlated with the response to immunotherapy and different TMEs, providing new insights into therapeutic strategies for cervical cancer. Nevertheless, a comprehensive study of the relationship between the overall landscape of PCD and immunotherapy in cervical cancer is lacking.

PCD plays a crucial role in the interaction between tumor development and tumor immunotherapy modulation [8, 23]. A growing body of evidence suggests that PCD is significantly correlated with prognosis and therapeutic strategies in a variety of cancers [24, 25]. For example, Zou et al. emphasized the critical role of PCD in the prognosis and treatment of triple-negative breast cancer [8]. Similarly, Qin et al. revealed the link between PCD and mitochondrial function in low-grade glioma (LGG) as a way to construct a prognostic model for LGG [26]. In addition, enhancing the response to anticancer immunotherapy by inducing PCD has emerged as a potential strategy to overcome resistance to targeted therapy and chemotherapy [27]. However, studies of PCD in cervical cancer have mainly focused on necroptosis [28], ferroptosis [29], autophagy [30], and cuproptosis [31]. With ongoing research, the number of genes associated with programmed cell death (PCD) continues to expand. Unlike previous studies, our research innovatively evaluated genes related to 18 distinct PCD modalities using single-cell data. This single-cell analysis allows for a deeper understanding of variations in PCD scores across different cell types, providing a more granular and precise perspective. By leveraging single-cell data, our study not only identifies cell-specific PCD patterns but also offers novel insights into the heterogeneity of PCD mechanisms, representing a significant advancement over earlier population-level analyses. In the prognostic model trained on TCGA data, the AUC values outperformed those from GEO datasets, though neither reached the threshold of 0.8—a benchmark typically associated with robust model specificity and sensitivity. Achieving this standard can prove particularly challenging in complex biological contexts or with heterogeneous datasets. The observed discrepancy between TCGA and GEO performance may stem from inherent differences in the training cohorts, such as variations in sample size, clinical characteristics, or data quality. Expanding the analysis to include additional datasets could enhance the model's accuracy and generalizability. Furthermore, the 5-year ROC results were notably lower than the 1- and 3-year outcomes. This decline might reflect limitations in the GEO dataset, including insufficient sample size or truncated follow-up durations.

In this study, we constructed a prognostic assessment model of CESC by identifying six PCD score-related genes (CD46, TFRC, PGK1, GNG5, GAPDH, and PLAU). CD46, also known as membrane cofactor protein (MCP), is a type I membrane protein that not only protects host cells from complement-dependent cytotoxicity (CDC) by inactivating C3b and C4b but also acts as a receptor for certain adenoviruses (Ad) and measles virus (MeV) [32]. Interestingly, recent studies have revealed that CD46 plays a pivotal role in the growth and metastasis of various solid tumors, including breast cancer, ovarian cancer, colorectal cancer, and bladder cancer [33–35]. Increasing evidence now suggests that targeting CD46

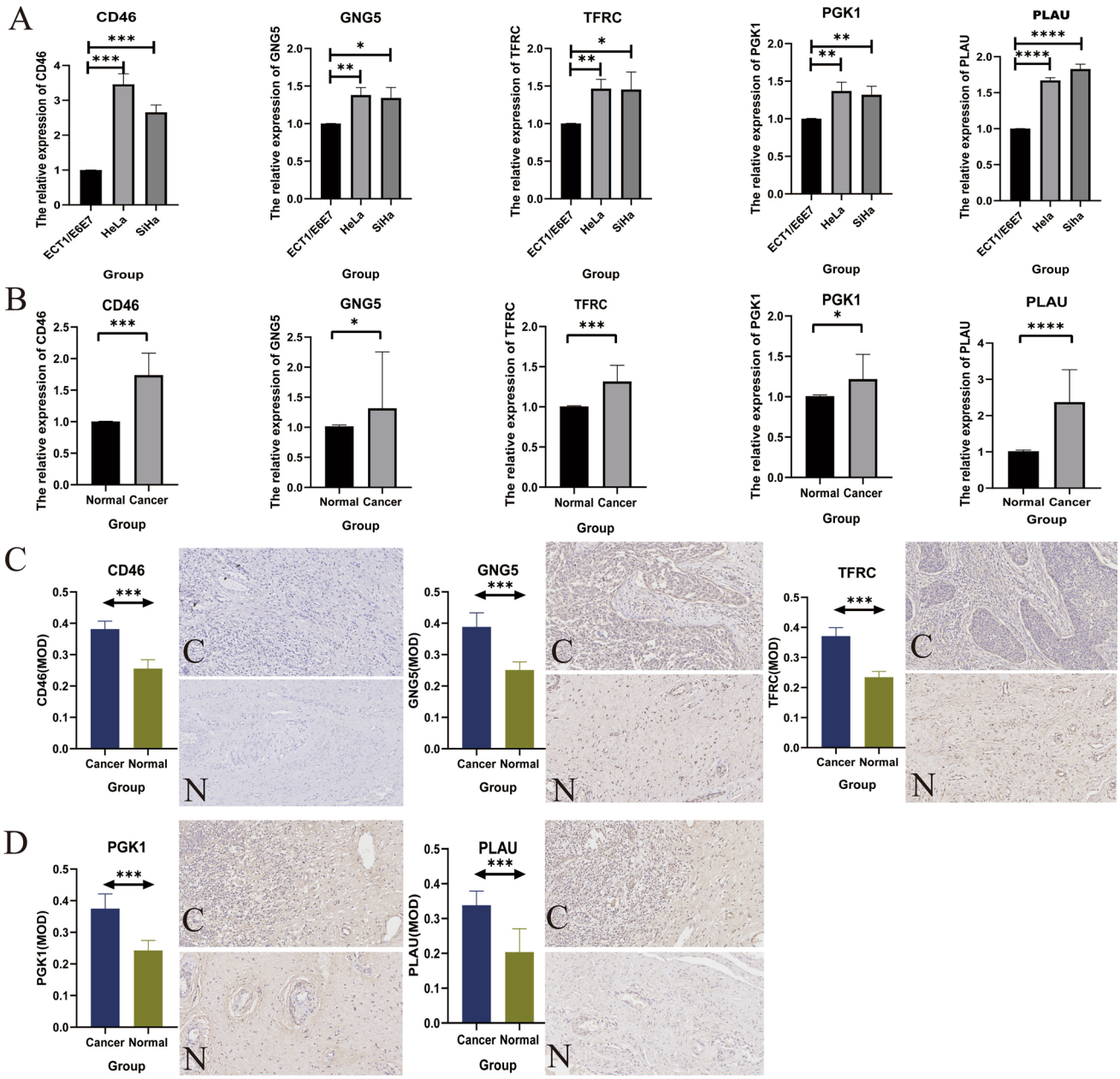

Fig. 11 External online database validation. **A** The expression of CD46, GNG5, TFRC, PGK1, and PLAU in cervical cancer cell line. **B** The expression of CD46, GNG5, TFRC, PGK1, and PLAU in cervical cancer patients. **C**,**D** The protein expression of CD46, GNG5, TFRC, PGK1, and PLAU in cervical cancer patients, respectively

could potentially be a therapeutic strategy for cancer. For instance, silencing CD46 expression via siRNA in vitro has been shown to enhance the sensitivity of cancer cells to CDC [36]. Moreover, downregulation of CD46 expression in cancer cells following treatment with therapeutic monoclonal antibodies can improve the efficacy of CDC and therapeutic outcomes [37]. CD46, a complement regulatory protein, plays a dual role in shaping the TME. By inhibiting complement-mediated tumor cell lysis, CD46 may protect cancer cells from immune destruction, thereby fostering an immunosuppressive milieu [38]. Additionally, CD46 signaling promotes the conversion of effector T cells into regulatory T cells (Tr1), further dampening anti-tumor immunity [39]. In mouse models of metastatic bladder cancer, targeted downregulation of CD46 has been found to induce protective anti-tumor $CD8^+$ T-cell responses [40]. Iron metabolism dysregulation, particularly excessive acquisition and retention of iron, has been implicated in tumorigenesis and cancer progression. TFRC, a type II transmembrane glycoprotein found in all nucleated cells, primarily functions to uptake iron by binding transferrin loaded with Fe^{3+} and subsequent endocytosis [41]. Growing evidence supports the notion that TFRC, as the most crucial iron

transporter for cellular iron uptake, is significantly dysregulated in many cancers, including cervical cancer, and plays a critical role in tumor initiation and development [42]. Abnormal expression of TFRC has also been observed in other female reproductive system cancers. In endometrial cancer, selective splicing of TFRC can lead to resistance of tumor cells to iron ions [43]. Furthermore, in ovarian cancer, TFRC promotes the proliferation and metastasis of epithelial ovarian cancer cells [44]. TFRC, a critical iron uptake mediator, influences immune infiltration through metabolic competition [45]. By sequestering iron, TFRC may starve tumor-infiltrating lymphocytes (TILs), impairing their effector functions. Moreover, TFRC modulates macrophage polarization by regulating iron availability, favoring the pro-tumor M2 phenotype over anti-tumor M1 macrophages [46]. PGK1, a gene closely related to metabolism, is highly anticipated [47]. PGK1 can synergize with glycolysis to promote tumor development [48]. PGK1 methylation in colorectal cancer promotes glycolysis and tumorigenesis [49]. PGK1 is also closely related to macrophages and can promote renal clear cell carcinoma and drug resistance through CXCR4 inflammatory factor [50, 51]. Some studies found that in cervical cancer HOXA1 can directly induce PGK1 expression, which in turn regulates glycolysis involved in cervical carcinogenesis [52]. In glioma, GNG5 [53] can promote tumor cell migration, proliferation, and correlate with poor prognosis of patients; the same role of promoting tumor development was found in lung cancer [54, 55]. Furthermore, it has been observed that PLAU is associated with cell migration and invasion in cervical cancer [56]. These results suggest that most of the characterized genes in this study are associated with cancer progression and have potential value in predicting patient prognosis.

The comprehensive analysis of this study based on the prognostic model found that patients in the low-risk group had a better prognosis compared with those in the high-risk group, which may be closely related to the fact that the low-risk group had higher immune function scores, higher immune scores, and immune cell infiltration. $CD8^+$ T cells in TME are well known antitumor immune cells that modulate the anticancer response to cytokines and are one of the indicators for assessing the efficacy of immunotherapy in patients [57]. Immune cells such as T-lymphocytes and macrophages in the tumor immune microenvironment can exhibit drug resistance through different accumulation of cytokines [58]. Immunotherapy is an important treatment modality for advanced cervical cancer, and Heeren et al. [20] found that TILs combined with anti-pd1 significantly improved the prognosis of metastatic cervical cancer. However, only a small proportion of patients with squamous cell carcinoma of the cervix (SCC) derive clinical benefit from ICB therapy [59]. Therefore, it is particularly important to identify immunotherapy-sensitive indicators. In this study, we found that low-risk patients had lower TIDE and Exclusion scores compared with the high-risk group, four IPS scores were higher in the low-risk group, and multiple immune checkpoint inhibitor genes, including PDCD1 and CTLA, were highly expressed in the low-risk group.

Several limitations of this study should be acknowledged. First, although the prognostic value and immunotherapy relevance of PCD-related genetic markers were validated by dividing TCGA data into different cohorts, external datasets are required to further confirm their reliability and accuracy before clinical application. A notable concern is the predominance of American populations in the TCGA database, which may introduce racial disparities when applied to other regions, such as Asia or Africa. To address this limitation, future studies should incorporate diverse cohorts from multiple geographic and ethnic backgrounds to ensure the generalizability of our findings. Additionally, the validation of genes was limited to a small dataset, emphasizing the need for larger clinical cohorts to verify the identified molecular subtypes and prognostic features. The inclusion of multi-center studies with standardized protocols would enhance the robustness and reproducibility of our results. Furthermore, in-depth in vitro and in vivo studies, including Western blotting, flow cytometry, immunofluorescence, and immunohistochemistry, are essential to elucidate the potential mechanisms of PCD-related genes in cervical cancer progression and immunotherapy. These mechanistic studies would not only validate our findings but also provide insights into the biological pathways underlying PCD-associated features, thereby facilitating the development of targeted therapeutic strategies.

5 Conclusion

In conclusion, this study is the first to comprehensively analyze 18 different PCD patterns and construct PCD-related characteristics of cervical cancer patients, which provides new indicators for predicting the efficacy and prognosis of therapeutic interventions in cervical cancer patients. Importantly, we found that patients associated with high CDI exhibited poor prognosis, advanced clinicopathologic staging, and relative insensitivity to immunotherapy, which may be related to the downregulation of TLSs. These findings highlight the clinical significance of PCD-associated features and offer novel insights for guiding individualized treatment strategies in cervical cancer.

Furthermore, the PCD signature identified in this study has promising potential for clinical applications. For instance, it could serve as a valuable tool to guide immunotherapy decisions by identifying patients who are more likely to benefit from immune checkpoint inhibitors. Additionally, the PCD signature may help stratify high-risk patients who require more aggressive treatment regimens, thereby improving clinical outcomes. These applications underscore the translational value of our findings and pave the way for future research aimed at optimizing therapeutic interventions for cervical cancer patients.

Acknowledgements None.

Author contributions Y.J.L. and Y.L: Investigation, Methodology, Validation, Writing-Original Draft, Funding Acquisition, Writing-Review & Editing. C.H.P: Review & Editing. X.F.L.: Resources, Supervision.

Funding This study was partially funded by the self-funded project of Guangxi Health Commission (Grant No. Z-A20231188).

Data availability All data generated or analyzed during this study can be obtained directly by contacting the corresponding author (Y.L.).

Code availability Further enquiries can be directed to the corresponding author.

Declarations

Ethics approval and consent to participate The clinical samples involved were approved by the Ethics Committee of the Second People's Hospital of Nanning. The data used in this study were obtained from public databases, therefore no additional ethical certification was required.

Consent for publication Not applicable.

Competing interests The authors declare no competing interests.

References

1. Bray F, Laversanne M, Sung H, et al. Global cancer statistics 2022: GLOBOCAN estimates of incidence and mortality worldwide for 36 cancers in 185 countries. CA Cancer J Clin. 2024;74(3):229–63.
2. Siegel RL, Miller KD, Wagle NS, et al. Cancer statistics, 2023. CA Cancer J Clin. 2023;73(1):17–48.
3. Aviki EM, Chen L, Dessources K, et al. Impact of hospital volume on surgical management and outcomes for early-stage cervical cancer. Gynecol Oncol. 2020;157(2):508–13.
4. Abu-Rustum NR, Yashar CM, Arend R, et al. NCCN Guidelines® Insights: cervical cancer, version 1.2024. J Natl Compr Canc Netw. 2023;21(12):1224–33.
5. Adiga D, Eswaran S, Pandey D, et al. Molecular landscape of recurrent cervical cancer. Crit Rev Oncol Hematol. 2021;157: 103178.
6. Mutlu L, Tymon-Rosario J, Harold J, et al. Targeted treatment options for the management of metastatic/persistent and recurrent cervical cancer. Expert Rev Anticancer Ther. 2022;22(6):633–45.
7. Tower J. Programmed cell death in aging. Ageing Res Rev. 2015;23(Pt A):90–100.
8. Zou Y, Xie J, Zheng S, et al. Leveraging diverse cell-death patterns to predict the prognosis and drug sensitivity of triple-negative breast cancer patients after surgery. Int J Surg. 2022;107: 106936.
9. Muller GJ, Hasseldam H, Rasmussen RS, et al. Dexamethasone enhances necrosis-like neuronal death in ischemic rat hippocampus involving mu-calpain activation. Exp Neurol. 2014;261:711–9.
10. Liu J, Hong MJ, Li YJ, et al. Programmed cell death tunes tumor immunity. Front Immunol. 2022;13: 847345.
11. Liu XG, Nie LT, Zhang YL, et al. Actin cytoskeleton vulnerability to disulfide stress mediates disulfidptosis. Nat Cell Biol. 2023;25(3):404–14.
12. Tang DL, Kang R, VandenBerghe T, et al. The molecular machinery of regulated cell death. Cell Res. 2019;29(5):347–64.
13. Wang Y, Kanneganti TD. From pyroptosis, apoptosis and necroptosis to PANoptosis: a mechanistic compendium of programmed cell death pathways. Comput Struct Biotechnol J. 2021;19:4641–57.
14. Zhou B, Liu J, Kang R, et al. Ferroptosis is a type of autophagy-dependent cell death. Semin Cancer Biol. 2020;66:89–100.
15. Bertheloot D, Latz E, Franklin BS. Necroptosis, pyroptosis and apoptosis: an intricate game of cell death. Cell Mol Immunol. 2021;18(5):1106–21.
16. Mishra AP, Salehi B, Sharifi-Rad M, et al. Programmed cell death, from a cancer perspective: an overview. Mol Diagn Ther. 2018;22(3):281–95.

17. Tang D, Kang R, Berghe TV, et al. The molecular machinery of regulated cell death. Cell Res. 2019;29(5):347–64.
18. Liu C, Zhang M, Yan X, et al. Single-cell dissection of cellular and molecular features underlying human cervical squamous cell carcinoma initiation and progression. Sci Adv. 2023;9(4):eadd8977.
19. Woo SR, Fuertes MB, Corrales L, et al. STING-dependent cytosolic DNA sensing mediates innate immune recognition of immunogenic tumors. Immunity. 2014;41(5):830–42.
20. Heeren AM, Rotman J, Stam AGM, et al. Efficacy of PD-1 blockade in cervical cancer is related to a $CD8^{+}FoxP3^{+}CD25^{+}$ T-cell subset with operational effector functions despite high immune checkpoint levels. J Immunother Cancer. 2019;7(1):43.
21. Perez-Ruiz E, Melero I, Kopecka J, et al. Cancer immunotherapy resistance based on immune checkpoints inhibitors: targets, biomarkers, and remedies. Drug Resist Updat. 2020;53: 100718.
22. Pedersen JG, Madsen AT, Gammelgaard KR, et al. Inflammatory cytokines and ctDNA are biomarkers for progression in advanced-stage melanoma patients receiving checkpoint inhibitors. Cancers. 2020;12(6):1414.
23. Hsu SK, Li CY, Lin IL, et al. Inflammation-related pyroptosis, a novel programmed cell death pathway, and its crosstalk with immune therapy in cancer treatment. Theranostics. 2021;11(18):8813–35.
24. Sha Y, Jiang R, Miao Y, et al. The pyroptosis-related gene signature predicts prognosis and indicates the immune microenvironment status of chronic lymphocytic leukemia. Front Immunol. 2022;13: 939978.
25. Feng S, Wang Z, Zhang H, et al. Identification of prognostic biomarkers for cervical cancer based on programmed cell death-related genes and assessment of their immune profile and response to drug therapy. J Gene Med. 2023;26(1): e3643.
26. Qin H, Abulaiti A, Maimaiti A, et al. Integrated machine learning survival framework develops a prognostic model based on inter-cross-talk definition of mitochondrial function and cell death patterns in a large multicenter cohort for lower-grade glioma. J Transl Med. 2023;21(1):588.
27. Yu J, Wang Q, Zhang X, et al. Mechanisms of neoantigen-targeted induction of pyroptosis and ferroptosis: from basic research to clinical applications. Front Oncol. 2021;11: 685377.
28. Yang Z, Li J, Tang Y, et al. Identification and validation a necroptosis-related prognostic signature in cervical cancer. Reprod Sci. 2023;30(6):2003–15.
29. Han S, Wang S, Lv X, et al. Ferroptosis-related genes in cervical cancer as biomarkers for predicting the prognosis of gynecological tumors. Front Mol Biosci. 2023;10:1188027.
30. Shi H, Zhong F, Yi X, et al. Application of an autophagy-related gene prognostic risk model based on TCGA database in cervical cancer. Front Genet. 2020;11: 616998.
31. Kong X, Xiong Y, Xue M, et al. Identification of cuproptosis-related lncRNA for predicting prognosis and immunotherapeutic response in cervical cancer. Sci Rep. 2023;13(1):10697.
32. Li J, Huang T, Hua J, et al. CD46 targeted ^{212}Pb alpha particle radioimmunotherapy for prostate cancer treatment. J Exp Clin Cancer Res. 2023;42(1):61.
33. Geller A, Yan J. The role of membrane bound complement regulatory proteins in tumor development and cancer immunotherapy. Front Immunol. 2019;10:1074.
34. Ni Choileain S, Hay J, Thomas J, et al. TCR-stimulated changes in cell surface CD46 expression generate type 1 regulatory T cells. Sci Signal. 2017;10:502.
35. Kemper C, Verbsky JW, Price JD, et al. T-cell stimulation and regulation: with complements from CD46. Immunol Res. 2005;32:31–43.
36. Geis N, Zell S, Rutz R, et al. Inhibition of membrane complement inhibitor expression (CD46, CD55, CD59) by siRNA sensitizes tumor cells to complement attack in vitro. Curr Cancer Drug Targets. 2010;10(8):922–31.
37. Wang H, Koob T, Fromm JR, et al. CD46 and CD59 inhibitors enhance complement-dependent cytotoxicity of anti-CD38 monoclonal antibodies daratumumab and isatuximab in multiple myeloma and other B-cell malignancy cells. Cancer Biol Ther. 2024;25(1):2314322.
38. Buettner R, Huang M, Gritsko T, et al. Activated signal transducers and activators of transcription 3 signaling induces CD46 expression and protects human cancer cells from complement-dependent cytotoxicity. Mol Cancer Res. 2007;5(8):823–32.
39. Le Buanec H, Gougeon ML, Mathian A, et al. IFN-alpha and CD46 stimulation are associated with active lupus and skew natural T regulatory cell differentiation to type 1 regulatory T (Tr1) cells. Proc Natl Acad Sci USA. 2011;108(47):18995–9000.
40. Varela JC, Imai M, Atkinson C, et al. Modulation of protective T cell immunity by complement inhibitor expression on tumor cells. Can Res. 2008;68(16):6734–42.
41. Jung M, Weigert A, Mertens C, et al. Iron handling in tumor-associated macrophages—is there a new role for lipocalin-2? Front Immunol. 2017;8:1171.
42. Buas MF, Rho J-H, Chai X, et al. Candidate early detection protein biomarkers for ER+/PR+ invasive ductal breast carcinoma identified using pre-clinical plasma from the WHI observational study. Breast Cancer Res Treat. 2015;153(2):445–54.
43. Zhang J, Chen S, Wei S, et al. CircRAPGEF5 interacts with RBFOX2 to confer ferroptosis resistance by modulating alternative splicing of TFRC in endometrial cancer. Redox Biol. 2022;57: 102493.
44. Yan Z, Duan C, Li X, et al. circ-TFRC downregulation suppresses ovarian cancer progression via miR-615-3p/IGF2 axis regulation. Cancer Cell Int. 2024;24(1):152.
45. Shang X, Wang H, Gu J, et al. Ferroptosis-related gene transferrin receptor protein 1 expression correlates with the prognosis and tumor immune microenvironment in cervical cancer. PeerJ. 2024;12: e17842.
46. Sun JL, Zhang NP, Xu RC, et al. Tumor cell-imposed iron restriction drives immunosuppressive polarization of tumor-associated macrophages. J Transl Med. 2021;19(1):347.
47. Fu Q, Yu Z. Phosphoglycerate kinase 1 (PGK1) in cancer: a promising target for diagnosis and therapy. Life Sci. 2020;256: 117863.
48. Nie H, Ju H, Fan J, et al. *O*-GlcNAcylation of PGK1 coordinates glycolysis and TCA cycle to promote tumor growth. Nat Commun. 2020;11(1):36.
49. Liu H, Chen X, Wang P, et al. PRMT1-mediated PGK1 arginine methylation promotes colorectal cancer glycolysis and tumorigenesis. Cell Death Dis. 2024;15(2):170.
50. Zhang Y, Yu G, Chu H, et al. Macrophage-associated PGK1 phosphorylation promotes aerobic glycolysis and tumorigenesis. Mol Cell. 2018;71(2):201-215.e7.

51. He Y, Wang X, Lu W, et al. PGK1 contributes to tumorigenesis and sorafenib resistance of renal clear cell carcinoma via activating CXCR4/ERK signaling pathway and accelerating glycolysis. Cell Death Dis. 2022;13(2):118.
52. Zhang Z, Peng J, Li B, et al. HOXA1 promotes aerobic glycolysis and cancer progression in cervical cancer. Cell Signal. 2023;109: 110747.
53. Zhang W, Liu Z, Liu B, et al. GNG5 is a novel oncogene associated with cell migration, proliferation, and poor prognosis in glioma. Cancer Cell Int. 2021;21(1):297.
54. Peng J, Li S, Li B, et al. Exosomes derived from M1 macrophages inhibit the proliferation of the A549 and H1299 lung cancer cell lines via the miRNA-let-7b-5p-GNG5 axis. PeerJ. 2023;11: e14608.
55. Zeng Y, Xiao D, He H, et al. SERINC2-knockdown inhibits proliferation, migration and invasion in lung adenocarcinoma. Oncol Lett. 2018;16(5):5916–22.
56. Gao Y, Ma X, Lu H, et al. PLAU is associated with cell migration and invasion and is regulated by transcription factor YY1 in cervical cancer. Oncol Rep. 2023;49(2):25.
57. Raskov H, Orhan A, Christensen JP, et al. Cytotoxic $CD8^+$ T cells in cancer and cancer immunotherapy. Br J Cancer. 2021;124(2):359–67.
58. Wu T, Dai Y. Tumor microenvironment and therapeutic response. Cancer Lett. 2017;387:61–8.
59. Doukuni R, Kobori T, Tanaka C, et al. Moesin serves as scaffold protein for PD-L1 in human uterine cervical squamous carcinoma cells. J Clin Med. 2022;11(13):3830.